Journal of Power Sources 274 (2015) 8–14

Contents lists available at ScienceDirect

Journal of Power Sources

journal homepage: www.elsevier.com/locate/jpowsour

A tightly integrated sodium titanate-carbon composite as an anode material for rechargeable sodium ion batteries

Zichao Yan, Li Liu*, Hongbo Shu, Xiukang Yang, Hao Wang, Jinli Tan, Qian Zhou, Zhifeng Huang, Xianyou Wang*

Key Laboratory of Environmentally Friendly Chemistry and Applications of Ministry of Education, School of Chemistry, Xiangtan University, Xiangtan 411105, Hunan, China

HIGHLIGHTS

- $Na_2Ti_3O_7$/C composite was firstly investigated.
- $Na_2Ti_3O_7$/C composite showed much better electrochemical performance than bare $Na_2Ti_3O_7$.
- $Na_2Ti_3O_7$/C composite is promising anode materials for sodium ion batteries.

ARTICLE INFO

Article history:
Received 22 July 2014
Received in revised form
5 October 2014
Accepted 6 October 2014
Available online 14 October 2014

Keywords:
Sodium ion batteries
Sodium titanate
Carbon
Anode
Composite

ABSTRACT

A novel sodium titanate-carbon ($Na_2Ti_3O_7$/C) composite has been successfully synthesized via a rheological phase method. The homogeneous-dispersed carbon not only sheathes the single $Na_2Ti_3O_7$ particle but also combines all individual $Na_2Ti_3O_7$ particles to a stable union, as characterized by X-ray diffraction, scanning electron microscopy (SEM), and high-resolution transmission microscopy (HRTEM). The uniformly distributed carbon forms a good network of electrically conductive paths among the $Na_2Ti_3O_7$ particles, which is closely interlinked with each other. So $Na_2Ti_3O_7$ active material can get electrons from all directions and be fully utilized for sodium ion insertion and extraction reactions, which can improve sodium storage properties with enhanced rate capability and super cycling performance. The $Na_2Ti_3O_7$/C composite exhibits much better electrochemical performance than bare $Na_2Ti_3O_7$, which displays a stable discharge capacity of 111.8 mAh g^{-1} at 1C after 100 cycles, while only 48.6 mAh g^{-1} for bare $Na_2Ti_3O_7$ at the same conditions. Furthermore, the composite shows relatively stable storage capacities during long term cycling even at 5C. The remarkably improved cycling performance and rate capability of $Na_2Ti_3O_7$ are attributed to the tight integration between carbon and $Na_2Ti_3O_7$ which may enhance the electronic conductivity, decrease the charge transfer resistance and improve the electrochemical stability during cycling, thus making a compelling case for its development as an advanced anode material for sodium ion batteries.

1. Introduction

Renewable energy storages as important energy storage devices for mobile, electric vehicle and portable applications have been attracted a great deal of awareness due to the environmental disruption and economic recession [1–3]. Cheaper, safer and more environmentally benign energy storage technologies have been considered as the most suitable candidate for the future renewable energy storages [4,5]. Compared with lithium ion batteries, sodium ion batteries (NIBs) with higher availability and potential for lower cost of raw materials have drawn scientists' attention [6–8]. However, the electrode material (especially the anode material) has been considered to be one of the main restrictions for the widely application of NIBs.

Sodium ion insertion into carbon anode materials was extensively studied by a lot of scientists. The results show that unless high pressures are used, sodium ion insertion into graphitic carbons is minimal [9–11]. Moreover, sodium metal cannot be used as the anode as well due to the possibility of dendrite formation and the low melting temperature of sodium metal from safety concerns [12]. In addition, hard carbon with high discharge capacity and good capacity retention also has been studied [13]. However, the

* Corresponding authors. Tel.: +86 731 58292206; fax: +86 731 58292477.
E-mail addresses: liulili1203@126.com (L. Liu), wxianyou@yahoo.com (X. Wang).

http://dx.doi.org/10.1016/j.jpowsour.2014.10.045
0378-7753/

low voltage discharge plateau between 0 and 0.1 V vs. Na/Na^+ could raise safety concerns that there may be sodium dendrite formation at such a low voltage range. So, it is of great urgency for us to find a perfect anode material for future NIBs. Various promising anode materials, such as $NiCo_2O_4$ [14], $Na_3V_2(PO_4)_3$ [15], Ni_3S_2 [16] and $NaFeF_3$ [17] have been fabricated to improve the applicability of NIBs. However, all of those reported anode materials have disadvantages, such as their high cost, environmentally unfriendly, complicated synthesis process or the charge/discharge voltage plateaus being unobvious.

Ti-based anode material with its inherent chemical stability, minimal toxicity, low cost, and high safety has been considered as one of the most suitable candidates for NIBs anode materials [18–20]. As a newly used anode material, sodium titanate, $Na_2Ti_3O_7$, with lower discharge plateau and abundant raw material resources has been studied as Na hosts. Senguttuvan et al. [21] were the first to report $Na_2Ti_3O_7$ as the anode materials for NIBs, and illustrated the proper potential of reversibly reaction in a discharge voltage region from 0.01 to 2.5 V. After that, Wang et al. [22] synthesized $Na_2Ti_3O_7$ rods via a reverse microemulsion method, and a reversible capacity of 72 mAh g^{-1} was achieved at 0.5C, but only 20 cycles were lasted. Pan et al. [23] synthesized layered $Na_2Ti_3O_7$ by a solid-state method. The layered $Na_2Ti_3O_7$ shows a reversible capacity of 85 mAh g^{-1} (0.5C) after 100 cycles, which indicates a good cycling stability. However, the $Na_2Ti_3O_7$ also suffers from structural distortion, low electronic conductivity and poor electrochemical stability upon sodium insertion/extraction, which may account for the low coulombic efficiency and continuous capacity fading of $Na_2Ti_3O_7$ electrodes [23]. Rudola et al. [24] prepared $Na_2Ti_3O_7$ particles via a solid-state method. The working electrode for sodium cell was fabricated by mixing the as-synthesized sample and carbon black via high-energy ball-milling process. The mixture electrode show good cycling performance. A reversible discharge capacity of 80 mAh g^{-1} can be retained after 100 cycles at 2C. However, it did not say more about the long-term cycling performance at high rates and the specific capability needed to be further improved. So it is not very encouraging just via high-energy ball-milling process reducing the grains size or mixing with conductive materials to solve the poor electrochemical stability of $Na_2Ti_3O_7$.

Forming a composite with carbon is an effective approach to increase the electronic conductivity, rate performance and cycling stability of the anode material for lithium ion batteries [25–27]. After the very few reports about the electrochemical activity of bare $Na_2Ti_3O_7$ in NIBs, there is no literature report on fabricating a tight integration of carbon and $Na_2Ti_3O_7$ to improve the electrochemical performance of $Na_2Ti_3O_7$. The effectiveness of the tight structure in improving the electrochemical performance of $Na_2Ti_3O_7$ is unknown. Based on the above points, it is of great significance to fabricate stable $Na_2Ti_3O_7$/C composite with high electrochemical activity in the view of both practical application and scientific research.

With the aim to synthesize the $Na_2Ti_3O_7$/C composite with stable and high electrochemical performance, we present a rheological phase method using anatase TiO_2 and Na_2CO_3 as raw material, glucose as carbon source. In this work, we successfully synthesized $Na_2Ti_3O_7$/C composite for the first time via this rheological phase method and illustrated its excellent electrochemical performance in NIBs.

2. Experimental

2.1. Synthesis of $Na_2Ti_3O_7$/C composite

$Na_2Ti_3O_7$/C composite was achieved via a rheological phase method (shown in Fig. 1). 0.5 g anatase TiO_2 spheres prepared by the soft-template method [28] and 0.23 g Na_2CO_3 (controlling the molar ratio of Na:Ti to 2:3) were milled in the alcohol. The obtained well blended suspension was then dried at 80 °C. A mixture of Na_2CO_3 and the anatase TiO_2 was preheated at 500 °C for 5 h, and then calcined at 750 °C for 8 h in air. The calcined product and glucose were blended homogeneously and then added into the alcohol to obtain a solid–liquid rheological mixture. After continuous magnetic stirring of the mixture for 2 h, it was dried at 80 °C for 4 h in a vacuum oven to eliminate ethanol adequately. Finally, the mixture was calcined at 600 °C for 3 h in a tubular furnace under argon gas protecting, with a heating rate of 5 °C min^{-1}, to form the $Na_2Ti_3O_7$/C composite. The mass ratio of $Na_2Ti_3O_7$ and glucose were settled as 2:1. According to the carbon residue of glucose after thermal treatment under argon gas protecting, the content of carbon in $Na_2Ti_3O_7$/C composite was about 5 wt.%. For comparison, bare $Na_2Ti_3O_7$ was also prepared in the same way except for the addition of glucose.

2.2. Structure and morphology characterization

The structures of the as-synthesized samples were characterized by X-ray diffraction. X-ray powder diffraction data were obtained using a Rigaku D/MAX-2500 powder diffractometer with a graphite monochromatic and Cu Kα radiation (λ = 0.15418 nm) operated at a scan rate of 5° min^{-1}. Scanning electron microscope (SEM) images of the samples were collected using a JEOL JSM-6610 scanning electron microscope, which were used to observe the morphology of the samples. Besides, high-resolution transmission electron microscopy (HRTEM) and fast-Fourier transform (FFT) measurements were carried out using a JEOL JEM-2100F transmission electron microscope at an acceleration voltage of 200 kV.

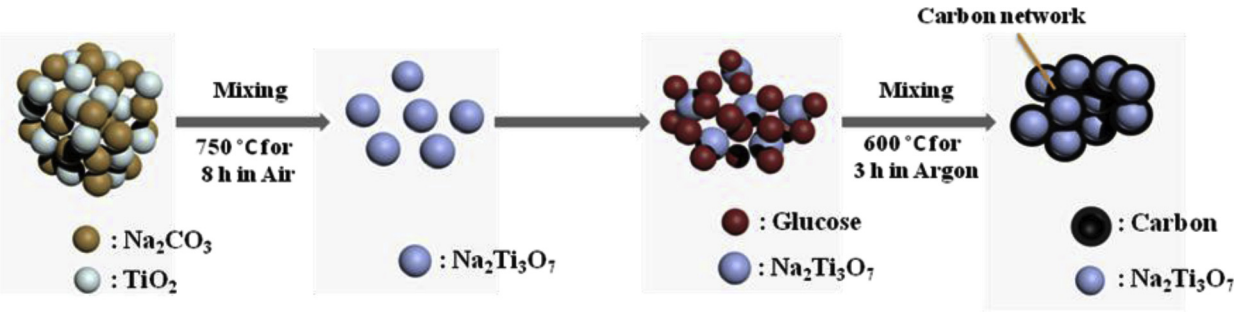

Fig. 1. Schematic illustration for the formation of $Na_2Ti_3O_7$/C composite's microstructure.

2.3. Electrochemical characterization

The working electrodes for sodium cells were fabricated by mixing the as-synthesized samples, carbon black, and Polyvinylidene fluoride (PVDF) binder with a weight ratio of 70:20:10 in *N*-methyl pyrrolidinone, which were then pasted on copper foil followed by drying under vacuum at 110 °C for 10 h. The average mass loading of the active material in the electrode was about 1.8 mg cm^{-2}. The testing cells were assembled with metallic sodium as the negative electrode, glass fiber separator (Whatman GF/F), and 1 M $NaClO_4$ in propylene carbonate (PC) electrolyte. The assembly of the testing cells was carried out in an argon-filled glove box, where water and oxygen concentration were kept less than 5 ppm. The charge–discharge cycle tests of NIBs (178 mA g^{-1} was assumed to be 1C rate) were run at different current densities between 0.01 and 2.5 V. All the cells were allowed to age for overnight before testing.

Cyclic voltammetry (CV) tests and EIS experiments were performed on a Zahner Zennium electrochemical workstation. CV tests were carried out at various scan rates on the potential interval 0.01–2.5 V (vs. Na^+/Na). The ac perturbation signal was ±5 mV and the frequency range was from 10 mHz to 100 KHz. All the tests were performed at room temperature.

3. Results and discussion

3.1. Characterization of $Na_2Ti_3O_7$/C composite

The X-ray diffraction (XRD) measurement was used to study the phase structure of the as-prepared samples. Fig. 2 presents the XRD patterns of anatase TiO_2 spheres, $Na_2Ti_3O_7$/C composite and $Na_2Ti_3O_7$. As shown in Fig. 2a, anatase TiO_2 spheres show good crystal structure, of which the diffraction peaks in the XRD pattern can be indexed well based on anatase phase of TiO_2 (JCPDS No. 21–1272). The inset of SEM image of anatase TiO_2 spheres shows a well distribution of homogeneous spheres with a diameter of 0.5 μm. In Fig. 2b, the as-prepared $Na_2Ti_3O_7$ shows good crystal structure, of which the diffraction peaks in the XRD pattern could be indexed well based on the $Na_2Ti_3O_7$ pattern corresponding to JCPDS No. 31-1329. For the $Na_2Ti_3O_7$/C composite, typical peaks at 10.5°, 15.8°, 25.6°, 43.8°, 47.7°, etc. can be found for monoclinic $Na_2Ti_3O_7$ structure. As we can see that both $Na_2Ti_3O_7$/C composite and $Na_2Ti_3O_7$ are in good agreement with the XRD pattern of monoclinic $Na_2Ti_3O_7$ structure. However, the peak intensity of $Na_2Ti_3O_7$/C composite is lower than that of $Na_2Ti_3O_7$, which can be greatly attributed to the introduction of carbon. This phenomenon is similar to other reports [29–31].

The morphology of $Na_2Ti_3O_7$ and $Na_2Ti_3O_7$/C composite are displayed in Fig. 3. As shown in Fig. 3a, the SEM image of $Na_2Ti_3O_7$ reveals the well distribution of homogeneous particles with relative smooth surface and diameters ranging from 0.2 to 0.8 μm. From the SEM image of $Na_2Ti_3O_7$/C composite (Fig. 3b), it is very clear that carbon as functional component wrap around the $Na_2Ti_3O_7$ particles, which may benefit for electrical conductivity and stability during cycling.

In order to further investigate morphology and structure of the final products, TEM and HRTEM images of $Na_2Ti_3O_7$ and $Na_2Ti_3O_7$/C composite are shown in Fig. 3c–f. TEM image in Fig. 3c presents the spherical particles of $Na_2Ti_3O_7$ with a diameter about 0.8 μm. From Fig. 3d, it can be found that $Na_2Ti_3O_7$ particle is well inserted in carbon. It is expected that such a combination may effectively avoids the structural distortion and enhances the capacity and stability of $Na_2Ti_3O_7$ electrodes upon sodium insertion/extraction. HRTEM (see Fig. 3e and f) analysis is employed to determine the crystal facets. Fig. 3e shows that $Na_2Ti_3O_7$ particles display clear crystal lattices, its fast-Fourier transform (FFT) image of the same region (inset) reveals that the diffraction spots have a lattice spacing related to the (011), (001), (200), (401) and (−112) planes, corresponding to monoclinic $Na_2Ti_3O_7$, which is in good agreement with the XRD results shown in Fig. 2. HRTEM image (Fig. 3f) taken on $Na_2Ti_3O_7$/C composite shows that the interplanar distance between adjacent lattice planes are 0.34 and 0.84 nm, corresponding to (001) and (011) planes of monoclinic $Na_2Ti_3O_7$. What's more, it also demonstrates that the homogeneous-dispersed carbon not only sheathes the single $Na_2Ti_3O_7$ particle but also combines all individual $Na_2Ti_3O_7$ particles to a stable union, which is well agree with the SEM image (Fig. 3b). Besides, the uniformly distributed carbon formed a good network of electrically conductive paths among the $Na_2Ti_3O_7$ particles, which are closely interlinked with each other. So active $Na_2Ti_3O_7$ material can get electrons from all directions and be fully utilized for sodium ion insertion and extraction reactions. All these above expect that the introduction of carbon might enhance electron transport and increase the stability of $Na_2Ti_3O_7$ particles.

3.2. Electrochemical analysis of $Na_2Ti_3O_7$/C composite

The electrochemical properties of $Na_2Ti_3O_7$/C composite as sodium insertion electrodes were studied in order to examine the effectiveness of the tight integration of carbon and $Na_2Ti_3O_7$ in improving the electrochemical performance of $Na_2Ti_3O_7$ electrode. Fig. 4a and b shows the cycle performance and charge/discharge profiles (insets) of $Na_2Ti_3O_7$ and $Na_2Ti_3O_7$/C composite at 1C. As shown in Fig. 4a, the discharge capacity of $Na_2Ti_3O_7$ drops from

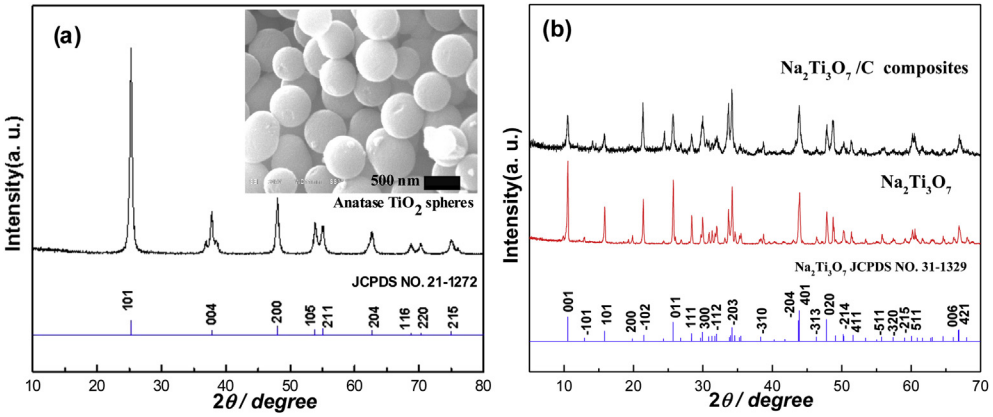

Fig. 2. XRD patterns of (a) anatase TiO_2 spheres, (b) $Na_2Ti_3O_7$/C composite and $Na_2Ti_3O_7$. The inset shows the corresponding SEM image of anatase TiO_2 spheres.

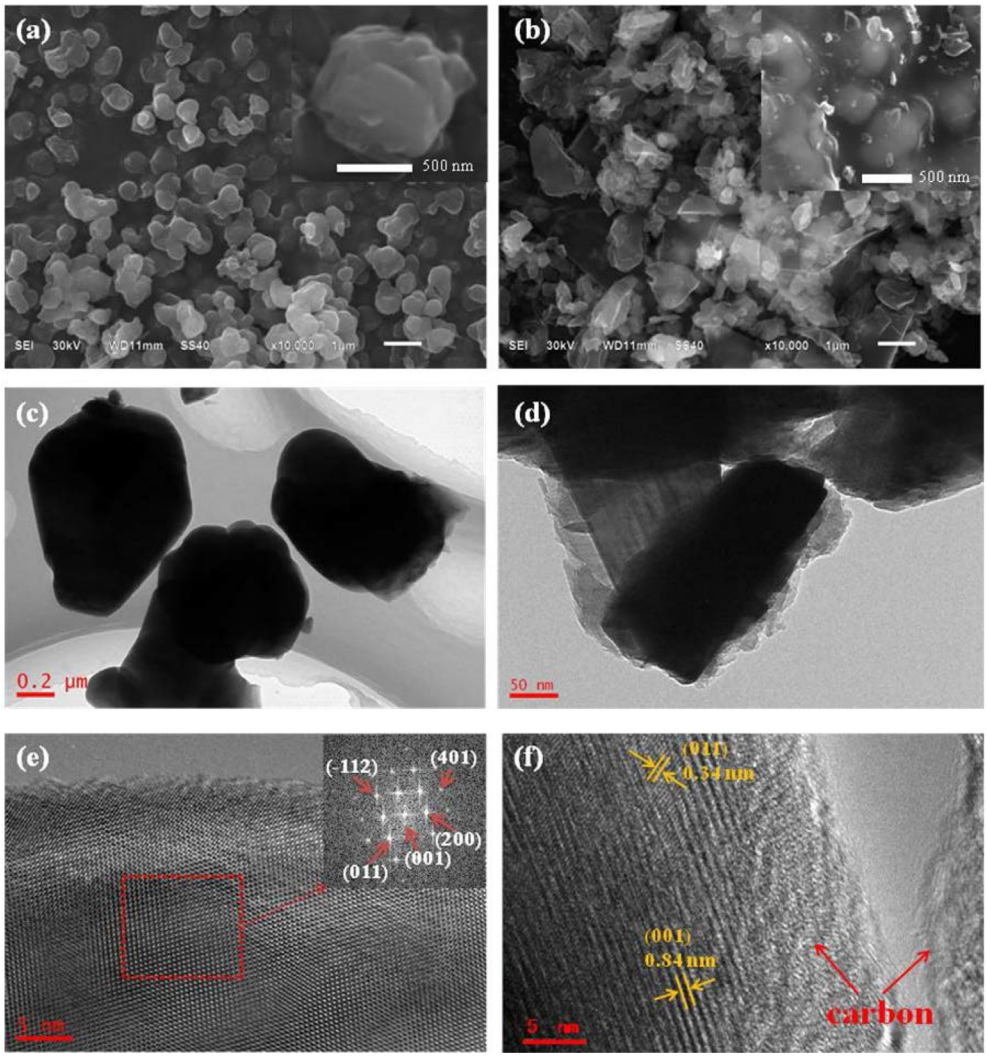

Fig. 3. SEM (a), TEM (c) and HRTEM (e) images of $Na_2Ti_3O_7$; SEM (b), TEM (d) and HRTEM (f) images of $Na_2Ti_3O_7$/C composite. The inset of HRTEM (e) shows the corresponding FFT pattern of $Na_2Ti_3O_7$.

279.6 to 48.6 mAh g^{-1} sharply after 100 cycles, with a large capacity loss of 82%. It is apparent that $Na_2Ti_3O_7$ shows a huge irreversible capacity loss on the first cycle and low capacity retention after 100 cycles. Interestingly, the huge capacity fading of $Na_2Ti_3O_7$ is ascribed to the first 10 cycles, which might be attributed to the instability caused by structure deformation during cycling [23]. However, the introduction of carbon improves the electrochemical performance of $Na_2Ti_3O_7$ remarkably. The carbon wrapping may avoid the direct contact of material and electrolyte, which effectively enhance the stability of $Na_2Ti_3O_7$ particles during the charge and discharge processes. $Na_2Ti_3O_7$/C composite can deliver discharge capacity of 276.2 mAh g^{-1} at the first discharge process, and the capacity of 111.8 mAh g^{-1} is finally remained after 100 cycles (see Fig. 4b). Moreover, with the increasing of the cycle numbers, the charge capacity of $Na_2Ti_3O_7$/C composite is getting stable and the coulombic efficiency is nearly 100% after the first several cycles. Compared with $Na_2Ti_3O_7$, the capacity of $Na_2Ti_3O_7$/C composite decreases in the initial cycle and it turns to be stable in the following cycles, which indicates a better cycling performance in NIBs. In order to exclude the effect from the carbon black additives, the relationship plot between specific capacity and cycle number for pure carbon black electrode in the range of 0.01 V–2.5 V at different rates in Na half-cells was utilized to present the sodium-storage performance of pure carbon black (see Fig S1 in Supporting information). The pure carbon black can deliver a high discharge capacity of 186.4 mAh g^{-1} at the first discharge process at 1C, and the capacity of 72.3 mAh g^{-1} is obtained in second cycle. And then a capacity below 50 mAh g^{-1} is remained after 20 cycles. A low discharge capacity of 25 mAh g^{-1} is obtained after 20 cycles at 5C. However, the $Na_2Ti_3O_7$/C composite shows much higher capacity than that of pure carbon black no matter at 1C (111.8 mAh g^{-1} after 100 cycles) or 5C (72.8 mAh g^{-1} after 100 cycles). Besides, the additive amount of carbon black that mixed in the electrode is only 20 wt.%. So, the capacity which provides by carbon black in Na half-cells can be ignored. Fig. 4a (insets) presents the voltage profiles of $Na_2Ti_3O_7$ at 1C. It exhibits very rapidly decreasing Ti redox plateaus (at ~ 0.3 V during discharge and 0.5 V during charging) after initial 10 cycles. However, the reversibility of Ti redox reactions has been well proved by Wang et al. [32]. Therefore, this phenomenon may account for the high rate cycling. The capacity retention data and voltage profiles of $Na_2Ti_3O_7$ at 0.2C were included for comparison. Fig. S2 illustrates that the Ti redox plateaus can be clearly observed at 0.2C even after 50 cycles. Fig. 4b (insets) shows the charge/discharge voltage profiles of $Na_2Ti_3O_7$/C composite for the 1st, 2nd, 10th, 30th, 40th, 50th, 80th and 100th cycles at 1C in the voltage range of 0.01–2.5 V. The

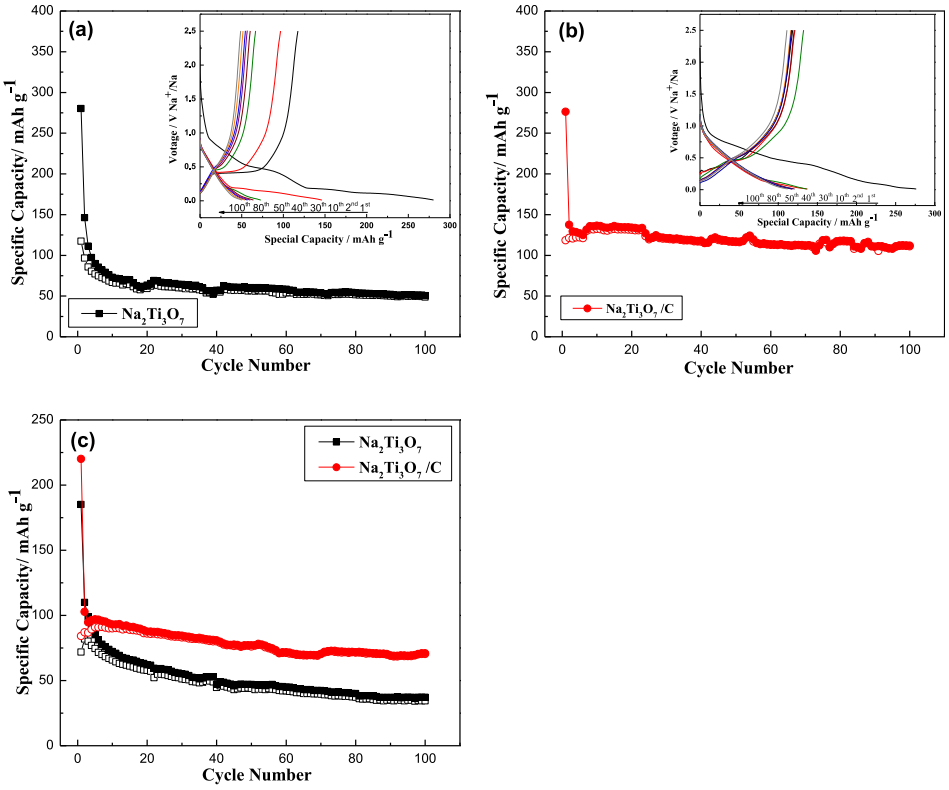

Fig. 4. Variation of charge (hollow) and discharge (solid) capacity versus cycle number and charge/discharge profiles (insets) for the (a) $Na_2Ti_3O_7$ and (b) $Na_2Ti_3O_7$/C composite at 1C (178 mA g^{-1}); (c) cycling performance of $Na_2Ti_3O_7$ and $Na_2Ti_3O_7$/C composite at 5C in the range of 0.01 V–2.5 V in Na half-cells.

sample shows sloped reaction plateaus locate at 0.47 V (charge) and 0.17 V (discharge), which is in accordance with the CV curves and delegates the representative charge/discharge profiles of $Na_2Ti_3O_7$ electrode in NIBs [22–24]. Besides, the carbon wrapping effectively prevents from the continuous capacity fading of $Na_2Ti_3O_7$ electrodes (especially for 2–10 cycles) which may account for the structural distortion of $Na_2Ti_3O_7$ electrodes upon sodium insertion/extraction [23]. The relationship plot between voltage and the insertion/extraction amount of Na during different cycles is shown in Fig. S3. The result reveals that its actual sodium content is relatively lower than the theoretical value (two sodium) except the first cycle. This might be ascribed to the reactions of SEI or other side reactions of the electrolyte deterioration in the initial cycle [23,24].

In order to further explore the effectiveness of the composited carbon in improving the electrochemical performance of $Na_2Ti_3O_7$ electrode, sodium cells made using $Na_2Ti_3O_7$ and $Na_2Ti_3O_7$/C composite were run at 5C for 100 cycles to test the long term cycling performance at high rate (Fig. 4c). Just like the electrochemical performance of $Na_2Ti_3O_7$ electrode at 1C, the second intensive decay of capacity from 2 to 10 cycles is also observed at 5C. The discharge capacity of $Na_2Ti_3O_7$ drops from 185.1 to 110 mAh g^{-1} after the first cycle, which can be connected with the irreversible capture of sodium ion, formation of the SEI (which is actually a heterogeneous multilayer) films and other side reactions during the first cycle [23,33,34]. And the capacity quickly drops to 67.8 mAh g^{-1} after 10 cycles due to the instability of $Na_2Ti_3O_7$ during the charge and discharge processes at high rate. After that, a poor capacity of 37 mAh g^{-1} is finally obtained after 100 cycles. However, the $Na_2Ti_3O_7$/C composite shows excellent stability during cycling. The capacity of $Na_2Ti_3O_7$/C composite starts at 220.1 mAh g^{-1} and still maintains at 95.3 mAh g^{-1} after 10 cycles. And then a high capacity of 72.8 mAh g^{-1} is finally obtained after 100 cycles, which is about twice the bare $Na_2Ti_3O_7$ electrode. The good cycling performance and high specific capacity at fast discharging/charging processes indicate the super structure stability of the $Na_2Ti_3O_7$/C composite during sodium insertion-extraction. In conclusion, $Na_2Ti_3O_7$/C composite performs much superior cycling stability and capacity retention than bare $Na_2Ti_3O_7$. These results suggest that the introduction of carbon greatly increases the conductivity and electrochemical stability of $Na_2Ti_3O_7$.

The rate capability of $Na_2Ti_3O_7$/C composite and $Na_2Ti_3O_7$ for NIBs was further investigated at various rates ranging from 0.5 to 5C as shown in Fig. 5. For each stage, the process was taken with 11 cycles. $Na_2Ti_3O_7$ can deliver discharge capacity of 97.6 mAh g^{-1}

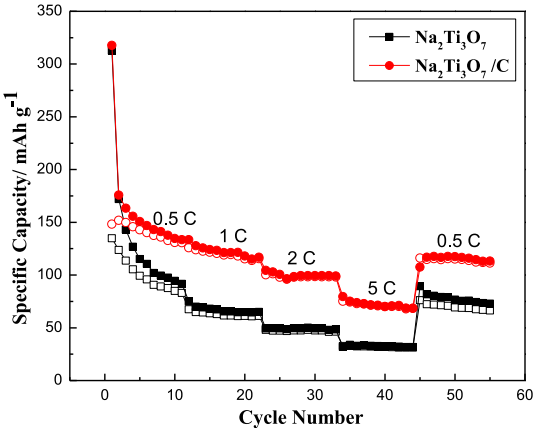

Fig. 5. Rate capability of $Na_2Ti_3O_7$ and $Na_2Ti_3O_7$/C composite at 0.5–5 C in the range of 0.01 V–2.5 V in Na half-cells. Charge (hollow) and discharge (solid).

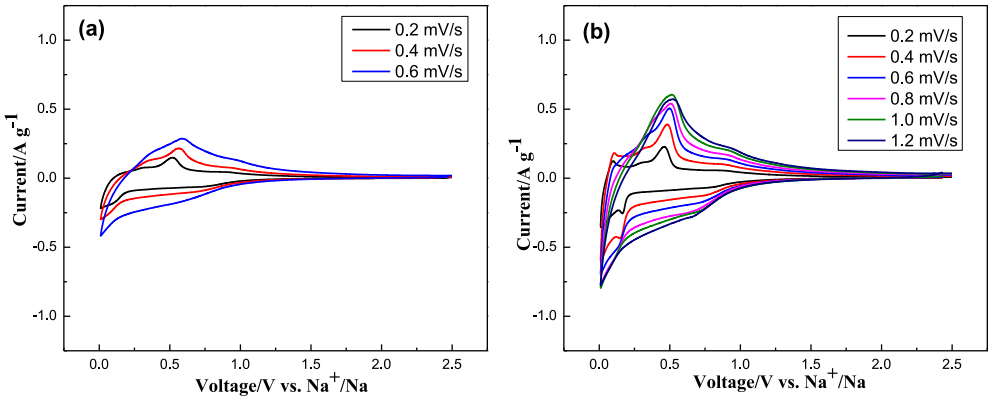

Fig. 6. CV plots for (a) $Na_2Ti_3O_7$ and (b) $Na_2Ti_3O_7$/C composite electrodes for the second cycle at various scan rates in a voltage window of 0.01–2.5 V.

at 0.5C. However, the specific discharge capacity sharply reduces to 64.7, 49.4 and 31.7 mA h g^{-1} at rates of 1C, 2C and 5C, respectively. After the high rate of 5C, the specific discharge capacity of 72.8 mAh g^{-1} is finally remained when reducing the rate to 0.5C. Clearly, $Na_2Ti_3O_7$/C composite has the better rate performance in capacities deliverable at various rates: the $Na_2Ti_3O_7$/C composite electrode is initially cycled at 0.5C where the capacity stabilized to 133.4 mA g^{-1} after 11 cycles. The rate is then increased to 1C, 2C and 5C. Stable discharge capacities of 121.2, 104.3 and 79.5 mAh g^{-1} are sustainable for 11 charge–discharge cycles at each of these rates. After deep cycling at high rates, a discharge capacity of 120.6 mAh g^{-1} is restored upon reducing the rate to 0.5C. Besides, the composites have excellent charge capacity retention even at high rates. The $Na_2Ti_3O_7$/C composite exhibits a remarkable rate capability, which is even superior to the performance of reported $Na_2Ti_3O_7$ rods [22] and $Na_2Ti_3O_7$ small platelets [24].

Since the higher capacity observed at high rates suggests a stability enhanced response, further investigations were performed using cyclic voltammetry. The CV curves of $Na_2Ti_3O_7$ and $Na_2Ti_3O_7$/C composite are shown in Fig. 6. It can be seen that the oxidation peak of bare $Na_2Ti_3O_7$ electrode (Fig. 6a) alters largely from 0.49 V to 0.59 V at different scan rates ranging from 0.2 mV s^{-1} to 0.6 mV s^{-1}, while the value of $Na_2Ti_3O_7$/C composite electrode (Fig. 6b) is 0.47 V at the scan rate of 0.2 mV s^{-1}, and alters slightly to 0.50 V when increasing the scan rate to 1.2 mV s^{-1}. This confirms the better reversibility and lower polarization of the $Na_2Ti_3O_7$/C composite electrode. Besides, a pair of redox peaks observed at 0.17 V (reduction peak) and 0.47 V (oxidation peak) remarkable appears at CV curves, which is in good agreement with the charge/discharge voltage profiles (see the insets in Fig. 4) and other reports [22,23]. However, it is interesting to note that the intensity of oxidation peak is higher than that of the reduction peak and the intensity of reduction peak is weakened with the increasing of the scan rates. This can be attributed to the more facile extraction process of the Na^+ ion upon charging at high rates comparing to the Na^+ ion insertion process during discharging, which has been clearly proved by other reports [23,24,35].

In order to explain the improved electrochemical performance of the composite, EIS measurement was introduced. The three-dimensional Nyquist plots of $Na_2Ti_3O_7$ and $Na_2Ti_3O_7$/C electrodes

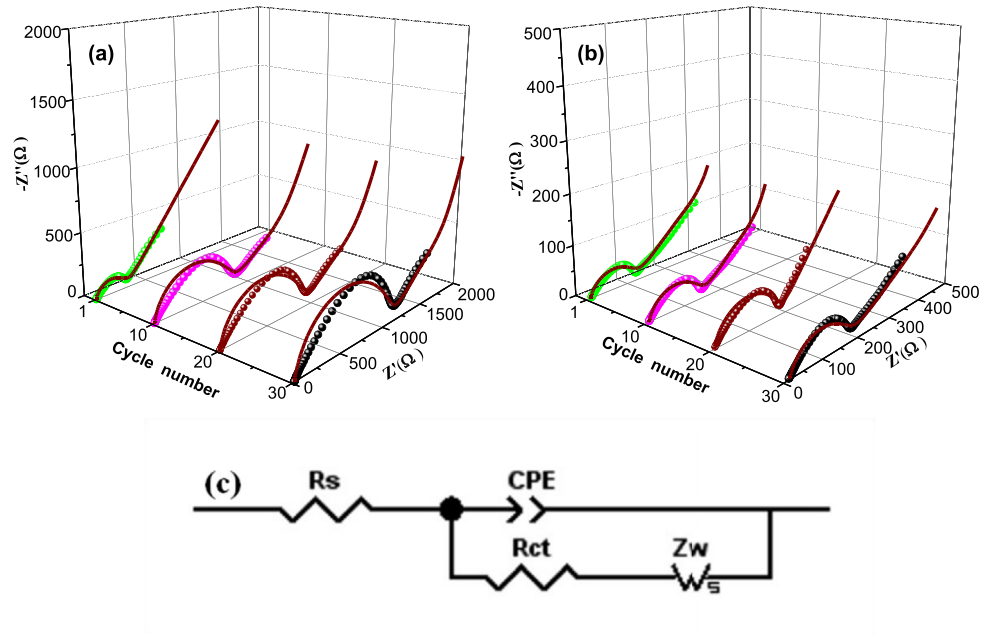

Fig. 7. Three-dimensional Nyquist plots measured for (a) $Na_2Ti_3O_7$ and (b) $Na_2Ti_3O_7$/C composite around 1.8 V after different numbers of cycling at 1C in Na half-cells; (c) the equivalent circuit model.

Table 1
R_s and R_{ct} values of $Na_2Ti_3O_7$ and $Na_2Ti_3O_7$/C composite after different cycles in Na half-cells.

Samples	R_s (Ω)				R_{ct} (Ω)			
	1st	10th	20th	30th	1st	10th	20th	30th
$Na_2Ti_3O_7$	13.2	18.2	20.7	25.5	260	760	870	1050
$Na_2Ti_3O_7$/C	10.8	11.1	11.5	13.6	122	130	150	172

after different numbers of cycling at around 1.8 V are shown in Fig. 7. The EIS is recorded during 1st to 30th charge/discharge cycles at room temperature. The shapes of the Nyquist plots for each cycle are similar. The EIS pattern is mainly composed of one semicircle in the high frequency region and a sloping line in the low frequency region (see Fig. 7a and b). Nyquist plots are fitted with the equivalent circuit model (see Fig. 7c), and the fitted impedance data are listed in Table 1. The fitting patterns show that fitting data are in well agreement with experimental data as shown in Fig. 7a and b. The equivalent circuit model includes the resistance of electrolyte (R_s), a constant phase element (CPE) associated with the interfacial resistance, and the semi-circle is correlated with the sodium charge transfer resistance at the interface R_{ct}. The linear portion is designated to Warburg impedance (Z_w), which is attributed to the diffusion of sodium ion into the bulk of the electrode materials. R_s denotes the solution resistances. It is explicit from Table 1 that the R_s values of $Na_2Ti_3O_7$/C composite are smaller than those of $Na_2Ti_3O_7$ at the same number of cycles, implying that the $Na_2Ti_3O_7$/C composite has lower structural distortion and the suppression of side reaction of electrolyte deterioration. The R_{ct} of $Na_2Ti_3O_7$ sample is 260 Ω after 1 cycle, and this value increases to 760 Ω after 10 cycles, which is consistent with the trend of huge capacity loss in the first 10 cycles. However, the R_{ct} of the $Na_2Ti_3O_7$/C sample is 122 Ω after 1 cycle, while this value only increases to 172 Ω after 30 cycles. It is well-known that the lower increase of charge transfer resistance during cycling means better cycle performance. These results are consistent with the excellent electrochemical performance of $Na_2Ti_3O_7$/C composite.

4. Conclusions

In summary, $Na_2Ti_3O_7$/C composite has been successfully synthesized via a rheological phase method. SEM and TEM measurements have confirmed that the $Na_2Ti_3O_7$ particle shows a pupa-like structure. The special structure combines all individual $Na_2Ti_3O_7$ particles together and forms a good network of electrically conductive paths among the $Na_2Ti_3O_7$ particles. Electrochemical tests show that the discharge capacity of $Na_2Ti_3O_7$/C composite still remain as high as 72.8 mAh g^{-1} after 100 cycles at the rate of 5C, while only 37 mAh g^{-1} for bare $Na_2Ti_3O_7$ at the same conditions. The excellent electrochemical performance of $Na_2Ti_3O_7$/C composite can be ascribed to tight integration of carbon and $Na_2Ti_3O_7$, which could enhance electronic conductivity, decrease the charge transfer resistance, and improve the electrochemical stability during cycling, as confirmed in CV, EIS and charge–discharge tests. All these results suggest that the $Na_2Ti_3O_7$/C composite can offer promising future for sodium ion battery anode materials.

Acknowledgments

This work is supported financially by the National Natural Science Foundation of China (Grant No. 51202209), Doctoral Fund of Ministry of Education of China (Grant No. 20114301120007), and Hunan Provincial Natural Science Foundation of China (Grant No. 14JJ6017).

Appendix A. Supplementary data

Supplementary data related to this article can be found at http://dx.doi.org/10.1016/j.jpowsour.2014.10.045.

References

[1] M. Shirpour, J. Cabana, M. Doeff, Energy Environ. Sci. 6 (2013) 2538.
[2] F.X. Wu, X.H. Li, Z.X. Wang, H.J. Guo, Nanoscale 5 (2013) 6936.
[3] J.S. Chen, Y.L. Tan, C.M. Li, Y.L. Cheah, D. Luan, S. Madhavi, F.Y.C. Boey, L.A. Archer, X.W. Lou, J. Am. Chem. Soc. 132 (2010) 6124.
[4] J.Y. Luo, Y.Y. Xia, Adv. Funct. Mater. 17 (2007) 3877.
[5] J.Y. Luo, W.J. Cui, P. He, Y.Y. Xia, Nat. Chem. 2 (2010) 760.
[6] V. Palomares, I. Villaluenga, K.B. Hueso, J. Carretero-Gonzalez, T. Rojo, Energy Environ. Sci. 5 (2012) 5884.
[7] M.D. Slater, D. Kim, E. Lee, C.S. Johnson, Adv. Funct. Mater. 23 (2013) 947.
[8] S. Li, Y.F. Dong, L. Xu, X. Xu, L. He, L.Q. Mai, Adv. Mater. 26 (2014) 3545.
[9] I.A. Udod, H.B. Orman, V.K. Genchel, Carbon 32 (1994) 101.
[10] S. Flandrois, B. Simon, Carbon 37 (1999) 165.
[11] H.T. Fang, M. Liu, D.W. Wang, T. Sun, D.S. Guan, F. Li, J.G. Zhou, T.K. Sham, H.M. Cheng, Nanotechnology 20 (2009) 227501.
[12] V.L. Chevrier, G. Ceder, J. Electrochem. Soc. 158 (2011) 1011.
[13] S. Komaba, W. Murata, T. Ishikawa, N. Yabuuchi, T. Ozeki, T. Nakayama, A. Ogata, K. Gotoh, K. Fujiwara, Adv. Funct. Mater. 21 (2011) 3859.
[14] R. Alćantara, M. Jaraba, P. Lavela, J.L. Tirado, Chem. Mater. 14 (2002) 2847.
[15] Z.L. Jian, L. Zhao, H.L. Pan, Y.S. Hu, H. Li, W. Chen, L.Q. Chen, Electrochem. Commun. 14 (2012) 86.
[16] J.S. Kim, H.J. Ahn, H.S. Ryu, D.J. Kim, G.B. Cho, K.W. Kim, T.H. Nam, J.H. Ahn, J. Power Sources 178 (2008) 852.
[17] Y. Yamada, T. Doi, I. Tanaka, S. Okada, J. Yamaki, J. Power Sources 196 (2011) 4837.
[18] Z. Bi, M.P. Paranthaman, P.A. Menchhofer, R.R. Dehoff, C.A. Bridges, M. Chi, B. Guo, X.G. Sun, S. Dai, J. Power Sources 222 (2013) 461.
[19] H. Zhang, X.P. Gao, G.R. Li, T.Y. Yan, H.Y. Zhu, Electrochim. Acta 53 (2008) 7061.
[20] Y. Sun, L. Zhao, H.L. Pan, X. Lu, L. Gu, Y.S. Hu, H. Li, M. Armand, Y. Ikuhara, L.Q. Chen, X.J. Huang, Nat. Chem. 4 (2013) 1870.
[21] P. Senguttuvan, G. Rousse, V. Seznec, J.M. Tarascon, M.R. Palacin, Chem. Mater. 23 (2011) 4109.
[22] W. Wang, C.J. Yu, Y.J. Liu, J.G. Hou, H.M. Zhu, S.Q. Jiao, RSC Adv. 3 (2013) 1041.
[23] H.L. Pan, X. Lu, X.Q. Yu, Y.S. Hu, H. Li, X.Q. Yang, L.Q. Chen, Adv. Energy Mater. 3 (2013) 1186.
[24] A. Rudola, K. Saravanan, C.W. Mason, P. Balaya, J. Mater. Chem. A 1 (2013) 2653.
[25] S.L. Jin, H.G. Deng, D.H. Long, X.J. Liu, L. Zhan, X.Y. Liang, W.M. Qiao, L.C. Ling, J. Power Sources 196 (2011) 3887.
[26] S.J. Park, Y.J. Kim, H. Lee, J. Power Sources 196 (2011) 5133.
[27] W.M. Zhang, X.L. Wu, J.S. Hu, Y.G. Guo, L.J. Wan, Adv. Funct. Mater. 18 (2008) 3941.
[28] S. Eiden-Assmann, J. Widoniak, G. Maret, Chem. Mater. 16 (2004) 6.
[29] J.J. Ding, Y.N. Zhou, Q. Sun, Z.W. Fu, Electrochem. Commun. 22 (2012) 85.
[30] M.M. Rahman, J.Z. Wang, M.F. Hassan, D. Wexler, H.K. Liu, Adv. Energy Mater. 1 (2011) 212.
[31] G.N. Zhu, H.J. Liu, J.H. Zhuang, C.X. Wang, Y.G. Wang, Y.Y. Xia, Energy Environ. Sci. 4 (2011) 4016.
[32] W. Wang, C. Yu, Z. Lin, J. Hou, H. Zhu, S. Jiao, Nanoscale 5 (2013) 594.
[33] Y. Xu, E.M. Lotfabad, H. Wang, B. Farbod, Z. Xu, A. Kohandehghan, D. Mitlin, Chem. Commun. 49 (2013) 8973.
[34] H.K. Han, T. Song, J.Y. Bae, L.F. Nazar, H.S. Kim, U. Paik, Energy Environ. Sci. 4 (2011) 1986.
[35] K. Tang, X. Yu, J. Sun, H. Li, X. Huang, Electrochim. Acta 56 (2011) 4869.